

Direct and real-time probing of both coherent and thermal lattice motions

H. Park, X. Wang, S. Nie, R. Clinite, J. Cao*

National High Magnetic Field Laboratory, Department of Physics, Florida State University, 1800 E. Paul Dirac Dr., Tallahassee, FL 32310, USA

Received 9 June 2005; received in revised form 18 July 2005; accepted 25 July 2005 by R. Merlin

Available online 16 August 2005

Abstract

We report direct measurement of laser-induced ultrafast structural dynamics on the atomic time and length scales in a 20-nm Al film by taking real-time snapshots of transmission electron diffraction patterns. The damped single-mode breathing motion of the Al film along the surface normal was recorded as coherent and in-phase oscillations of all the Bragg peak positions, which had a period of 6.4 ps. The concurrent lattice heating with a time constant of 630 fs was measured by tracking the associated Bragg peak intensity attenuation. These results suggest a direct approach to identify the mechanisms of laser-induced ultrafast solid–liquid phase transition, as well as thermal or non-thermal melting, via probing the temporal evolution of their diffraction patterns.

© 2005 Elsevier Ltd. All rights reserved.

PACS: 78.47.+p; 45.80+5; 46.40.-f; 63.20.-e

Keywords: A. Thin films; C. Electron diffraction; D. Phase transitions

1. Introduction

The studies aimed at direct observations of atom motions on the time scale of a single atomic vibration period (100 fs to ~ 1 ps) have been and are being carried out by many research groups using both ultrafast time-resolved X-ray [1–9] and electron diffraction [10–19] as a real-time structural probe. These studies are motivated by the fact that atomic motions on this fundamental time scale ultimately determine the genesis and evolution of new phases in solids, the kinetic pathways of chemical reactions, and the efficiencies and functions of biological processes. A thorough understanding of these dynamic behaviours on the time and length scales of

atomic motions provides the guiding principles to control these structural evolutions, which will have important scientific applications in solid-state physics, chemistry, biology and materials science.

The study of structural dynamics on this fundamental level requires directly monitoring the atomic motions on milli-ångström length scale and on the relevant time scale of 10^{-12} s or less. Previously, only femtosecond (fs) time-resolved optical measurements could provide adequate temporal resolution, albeit with indirect sensitivity of structural arrangement [20]. Recent developments in time-resolved diffraction have led to the capability of directly observing the laser-induced loss of long-range order [4,7,9,18,21]. However, a clear picture of lattice dynamics initiated by femtosecond optical excitation remains obscure. Here, we report a direct and real-time measurement of both coherent and thermal atomic motions in thin-film aluminium using femtosecond electron diffraction (FED). It showed a coherent

* Corresponding author. Tel.: +1 850 644 0527; fax: +1 850 644 5038.

E-mail address: jcao@magnet.fsu.edu (J. Cao).

lattice oscillation with a period of 6.4 ps starting immediately after optical excitation with concurrent lattice heating, reaching a final equilibrium temperature 1.9 ps later.

2. Experimental

The experiments were conducted on the femtosecond electron diffraction instrument [17], composed of an amplified Ti:Sapphire laser system, a femtosecond electron gun, a streak camera and a two-dimensional single electron detector. The output laser pulses, with ~ 50 -fs temporal duration and average pulse energy of up to 1 mJ centered at 790-nm wavelength, are first divided into pump and probe pulses by a beam splitter. The pump pulses, containing $\sim 90\%$ of original beam energy, are directed through a precision linear translation stage and used to initiate the structural dynamics. The remaining 10% optical pulses are sent through a frequency tripler. The tripled fs pulses, with photon energy of ~ 4.7 eV, are converted to fs electron pulses via photoemission and used to record the temporal evolutions of structural changes by taking snapshot of transmission diffraction patterns. The delay times between the excitation optical and the probe electron pulses are controlled by varying the relative optical path difference between the two beams.

The polycrystalline thin-film aluminium samples with nominal thickness of 20 ± 3.0 nm were prepared by thermal evaporation of Al in high vacuum on freshly cleaved NaCl single-crystal substrates. They were detached in a solvent and transferred to TEM grids as free-standing films. To ensure a uniform excitation of probed sample volume, the excitation optical beam size (~ 2 mm) was set about six times larger than that of the probe electron beam ($\sim 330 \mu\text{m}$). In each FED experiment, the electron pulse width was measured by a homemade streak camera. Assuming Gaussian shape, the electron pulse width is: $\Delta\tau_e = K_s \sqrt{W_{\text{str}}^2 - W_{\text{un}}^2}$, where K_s (~ 150 fs/pixel) is the streaking speed, and W_{str} and W_{un} are the respective full width at half maximum (FWHM) of electron beam sizes for streaked and un-streaked pulses. For the low electron beam intensity ($< 1000 e^-/\text{pulse}$) used in the experiment, the temporal pulse width was determined to be less than the 400-fs resolution of our streak camera. The overall temporal resolution, convoluting the excitation laser pulse width, probe electron pulse width and the temporal degradation [22], was less than 500 fs [17]. To avoid any possible sample damage after extended exposure to the pump laser pulses, the laser excitation fluence was kept lower than $3 \text{ mJ}/\text{cm}^2$. In addition, the diffraction patterns without the pump laser were also recorded at each time delay and used as a reference to correct any extraneous changes, such as electron beam walking and inherent long-term system drift.

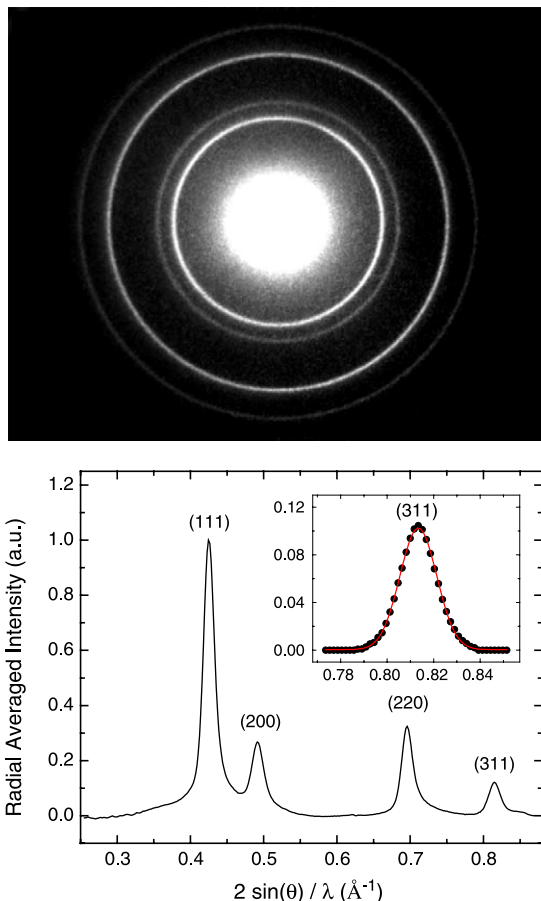


Fig. 1. Top panel: Diffraction pattern of polycrystalline free-standing thin-film aluminium of 20-nm thickness. It was recorded with $\sim 2 \times 10^7$ electrons and at $\sim 2.2 \text{ mJ}/\text{cm}^2$ laser excitation fluence. Bottom panel: The corresponding radial averaged intensity curve. Inset: A typical fit of (311) Bragg peak to a Gaussian profile. The peak center position was determined to be 0.81669 ± 0.00004 (\AA^{-1}) (470.99 ± 0.02 pixel).

3. Results and discussion

A typical diffraction pattern along with its intensity curve as a function of diffraction angle (momentum transfer $S = 2 \sin \theta / \lambda$) are shown in Fig. 1. The diffraction intensity curve was obtained by radially averaging a 2D diffraction pattern recorded with $\sim 2 \times 10^7$ electrons at 60 keV beam energy ($\lambda = 0.0487 \text{ \AA}$) and at $\sim 2.3 \text{ mJ}/\text{cm}^2$ laser excitation fluence. To obtain a quantitative measurement of structural dynamics, we fitted each Bragg peak with a Gaussian line profile (inset in the bottom panel of Fig. 1) to determine its peak center, which is defined as peak position, peak intensity and the peak FWHM. The data obtained with pump laser on were then normalized to that with laser blocked to eliminate any extraneous errors.

The temporal evolutions of (111) and (311) Bragg peak positions as a function of delay times are summarized in

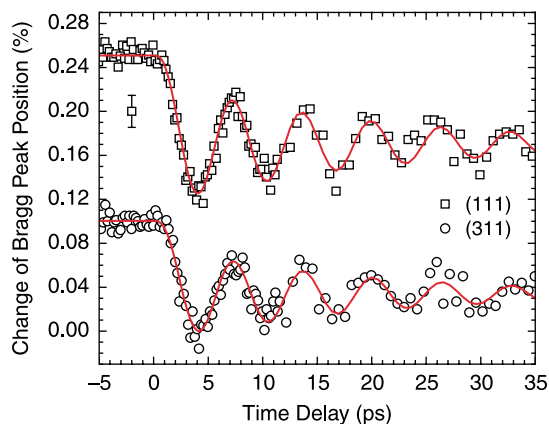


Fig. 2. Temporal evolution of (111) and (311) Bragg peak positions. Positive time delays correspond to probe electron pulses arriving after the excitation laser pulses. The error bars represent one standard deviation from the Gaussian peak profile fitting. Solid lines are fits to the data using a damped oscillator model.

Fig. 2. A few features are immediately noticeable. First, the Bragg peak starts an oscillatory motion centered at a newly established and reduced Bragg ring radius (expanded equilibrium lattice constant). Second, the vibration has a maximum displacement at time zero and displays a nearly cosine time dependence, indicating a displacive excitation mechanism [23]. Third, all Bragg peaks oscillate perfectly in-phase with one another with the same vibrational period. We fitted the vibration data with a damped oscillation formula [24] and obtained the same vibrational period of 6.4 ± 0.5 ps and damping time constant of 20 ± 2 ps for all the Bragg peaks to within one standard deviation. The Fourier transform of vibration data for the (311) Bragg ring gives a single peak centered at ~ 0.16 THz, which is in excellent agreement with a 6.4-ps vibration period and indicates only a single-mode of acoustic wave was launched. We also conducted power-dependent measurements and found that the vibration amplitude is proportional to the excitation laser fluence with no observable change of the vibrational period in the fluence range of 1.4–3 mJ/cm².

The Bragg peak oscillations observed with FED are correlated with the actual breathing motion of the Al film along the surface normal generated by the impulsive fs optical excitation. After excitation, the nearly uniform ultrafast heating across the thin-film induced from enhanced hot electron transport [25] and strong electron–phonon scattering [26] establishes a new, expanded, equilibrium lattice position in a time scale shorter than the lattice response time. Under this nearly impulsive and displacive excitation [23,27], a coherent lattice vibration (coherent longitudinal acoustic phonons) centered at the new equilibrium position was launched along the direction of surface normal. In the free-standing film with the open-boundary condition, a one-dimensional (1D) standing wave is formed with the corresponding vibrational period given

by, $T=2L/v$, where L is film thickness and v is the longitudinal sound velocity [5,28]. This breathing motion generates an uneven stretch and compression to the film along the surface normal, that is, the atoms at the center of the film remain stationary, while the atoms at the two open surfaces experience the biggest vibration. The uneven stretch will rotate the lattice planes towards the surface normal, which broadens the Bragg plane spacing accordingly and results in the contraction of Bragg peak radius. Conversely, the uneven film compression will decrease the inter-plane spacing, introducing the expansion of Bragg peak radius. In the diffraction pattern, this periodic film breathing motions will be exhibited as an oscillation of the Bragg ring radius for polycrystal films, as observed in FED. The vibrational period of 6.4 ps recorded with FED is in very good agreement with the 1D standing wave condition, by using the nominal average film thickness (L) of 20 ± 3.0 nm and sound velocity of 6420 m/s [29]. Importantly, the observed in-phase oscillation of all the Bragg peaks supports the single phonon mode resulting from nearly uniform film heating, and is distinct from the widely used surface heating excitation approach [28,30,31]. In surface heating, since the film thickness is much larger than the light penetration depth, thermal expansion into the film launches a longitudinal acoustic pulse propagating normal to the plane of the film with many wave vector components, up to the inverse of the optical excitation depth.

The above results also demonstrate the ability to determine the lattice constant change with sub-milli-ångström accuracy on ultrafast time scale with FED. For small angle diffraction with Bragg angle less than 1.6° in the current experiment, the relative change of linear Bragg peak position (Bragg ring radius $\Delta r/r$) recorded in the diffraction pattern equals the relative change of lattice plane spacing ($\Delta d/d$) according to Bragg's Law. This detection sensitivity of 0.02% relative Bragg peak position change corresponds to a spatial resolution less than a milli-ångström.

To gain a more complete picture of the lattice dynamics, we also measured the temporal evolution of thermal lattice motions (lattice temperature T_l) by monitoring the associated Bragg peak intensity attenuation with FED. The temporal evolution of lattice temperature measured with FED is displayed in Fig. 3. These data were obtained by first calculating the (311) peak intensity then normalizing to that of the (111) peak for each diffraction intensity curve at a given time delay. Then, this normalized intensity was converted to the lattice temperature using the Debye–Waller factor [32], calibrated by measuring the lattice expansion at its new equilibrium position and dividing it with the linear expansion coefficient of aluminium [29]. This approach is valid under the kinematical diffraction theory, which holds well in the current experiment considering that the mean free path for elastic scattering of 60 keV electrons in Al is more than 50 nm [33]. The time constant of $\tau_{e-ph} = 630 \pm 90$ fs for the lattice thermalization was obtained by fitting the data with an exponential function (solid line in the

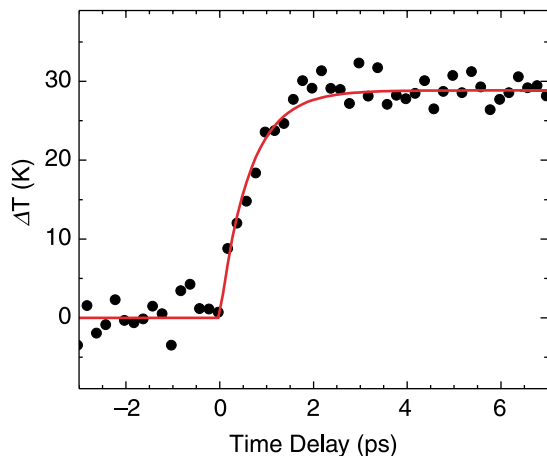


Fig. 3. Temporal evolution of lattice temperature as a function of delay times. The solid line is a fit to the data using an exponential function with a time constant $\tau_{e-ph} = 630 \pm 90$ fs.

Fig. 3). Importantly, the time for the lattice to reach its final equilibrium temperature (~ 1.9 ps) is comparable to one quarter of the vibrational period. At this time the coherent lattice vibration nearly reached its new equilibrium with highest vibration speed. These observations clearly show that the two modes of lattice motions, namely both coherent vibration and random thermal motions, are taking place concurrently after the optical excitation.

In contrast to the large intensity modulation in poly-atomic single crystals previously observed under strong excitation conditions [6,8], no Bragg peak intensity oscillation associated with coherent lattice vibration was detected under the current lower optical excitation. We believe that because Al is a mono-atomic crystal with only one atom per unit cell, the Bragg peak intensity (proportional to the square of structural factor) is solely determined by the atomic scattering factor. In general, this is a slow decaying function of diffraction angle [32]. Consequently, the intensity modulation induced by the coherent breathing lattice vibration is minimal, in contrast to the much larger intensity modulation arising from the large structural factor change due to the interference effect between different scattering centers in poly-atomic crystals [6,8].

The time constant of actual lattice thermalization (τ_{e-ph}) as measured by FED is several times longer than that predicted by our simulation using the two-temperature model (TTM) [34], the optical absorption depth of 7.4 nm [35] and the parameters for Al [26]. As pointed out by a previous study [26], by assuming instantaneous electron thermalization, TTM tends to significantly overestimate the e-ph coupling strength and predicts a much faster lattice heating rate. The lattice thermalization time measured with FED is in very good agreement with a more recent theoretical study using a refined model combining both TTM and molecular dynamics simulation [36] and a recent

measurement of ultrafast heating of Al using transient optical reflectivity, where approximately 2-ps lattice heating time was observed [37].

The results presented here provide a new approach to identify the mechanisms of laser-induced ultrafast solid-liquid phase transition, either thermal or non-thermal melting, by directly probing the different temporal evolution of their diffraction patterns. For laser-induced thermal melting, the phase transition proceeds by nucleation and subsequent cluster growth and the energy is transferred from electrons to the lattice in the form of heat. The time scale for this type of phase transition will be in the range of a few picoseconds [18,38], longer than the electron-phonon thermalization time. On this time scale, as shown in our results, large coherent lattice motions induced by the high excitation fluence required for melting will be launched before the solid elasticity has been destroyed by the melting. Accordingly, the temporal evolution of diffraction patterns will proceed with progressive Bragg peak shifting and concurrent intensity attenuation until the Bragg peak finally disappears due to the loss of long-range-order. In contrast, non-thermal melting is related to band structure collapse and lattice instability resulting from a strong electronic transition from bonding to anti-bonding states [39,40], so this melting will complete in a few hundred fs. Since no coherent lattice motions are involved, the diffraction patterns will only show continuous Bragg peak intensity attenuation with possible width broadening. Currently, the experiments for identifying these different melting pathways in polycrystalline Al thin-film under different excitation fluences are being conducted using the sub-ps single-shot diffraction equipment in our lab.

4. Conclusion

This work demonstrates the superior ability of femtosecond electron diffraction to study the transiently generated structural dynamics with sub-milli-ångström spatial resolution in real-time. In this instance, both coherent and random lattice motions were directly measured and differentiated, which provides a clear view of laser-induced lattice dynamics. The damped single-mode breathing motion of the Al film along the surface normal was recorded as the coherent oscillation of the Bragg peak positions with a period of 6.4 ps. The concurrent lattice temperature evolution with a time constant of 630 fs was measured by tracking the associated Bragg peak intensity attenuation. The results provide a new approach to identify the mechanisms of laser-induced ultrafast solid-liquid phase transition, as well as thermal or non-thermal melting, by directly probing the different temporal evolution of their diffraction patterns.

Acknowledgements

We would like to acknowledge the contributions of Dr Zhao Hao, Chenggang Tao, and Dr Florentin Popescu in developing our femtosecond electron diffraction setup. This work was supported by the Florida State University and the National Science Foundation by grant number DMR-0305519.

References

- [1] R.W. Schoenlein, W.P. Leemans, A.H. Chin, P. Volfbeyn, T.E. Glover, P. Balling, M. Zolotarev, K.J. Kim, S. Chattopadhyay, C.V. Shank, *Science* 274 (1996) 236–238.
- [2] C. Rischel, A. Rousse, I. Uschmann, P.A. Albouy, J.P. Geindre, P. Audebert, J.C. Gauthier, E. Forster, J.L. Martin, A. Antonetti, *Nature* 390 (1997) 490–492.
- [3] A.H. Chin, R.W. Schoenlein, T.E. Glover, P. Balling, W.P. Leemans, C.V. Shank, *Phys. Rev. Lett.* 83 (1999) 336–339.
- [4] C.W. Siders, A. Cavalleri, K. Sokolowski-Tinten, C. Toth, T. Guo, M. Kammler, M.H. von Hoegen, K.R. Wilson, D. von der Linde, C.P.J. Barty, *Science* 286 (1999) 1340–1342.
- [5] A. Cavalleri, C.W. Siders, F.L.H. Brown, D.M. Leitner, C. Toth, J.A. Squier, C.P.J. Barty, K.R. Wilson, K. Sokolowski-Tinten, M.H. von Hoegen, D. von der Linde, M. Kammler, *Phys. Rev. Lett.* 85 (2000) 586–589.
- [6] A.M. Lindenberg, I. Kang, S.L. Johnson, T. Missalla, P.A. Heimann, Z. Chang, J. Larsson, P.H. Bucksbaum, H.C. Kapteyn, H.A. Padmore, R.W. Lee, J.S. Wark, R.W. Falcone, *Phys. Rev. Lett.* 84 (2000) 111–114.
- [7] A. Rousse, C. Rischel, S. Fourmaux, I. Uschmann, S. Sebban, G. Grillon, P. Balcou, E. Foster, J.P. Geindre, P. Audebert, J.C. Gauthier, D. Hulin, *Nature* 410 (2001) 65–68.
- [8] K. Sokolowski-Tinten, C. Blome, J. Blums, A. Cavalleri, C. Dietrich, A. Tarasevitch, I. Uschmann, E. Forster, M. Kammler, M. Horn-von-Hoegen, D. von der Linde, *Nature* 422 (2003) 287–289.
- [9] A.M. Lindenberg, J. Larsson, K. Sokolowski-Tinten, K.J. Gaffney, C. Blome, O. Synnergren, J. Sheppard, C. Coleman, A.G. MacPhee, D. Weinstein, D.P. Lowney, T.K. Allison, T. Matthews, R.W. Falcone, A.L. Cavalieri, D.M. Fritz, S.H. Lee, P.H. Bucksbaum, D.A. Reis, J. Rudati, P.H. Fuoss, C.C. Kao, D.P. Siddons, R. Pahl, J. Als-Nielsen, S. Duesterer, R. Ischebeck, H. Schlarb, H. Schulte-Schrepping, T. Tschentscher, J. Schneider, D. von der Linde, O. Hignette, F. Sette, H.N. Chapman, R.W. Lee, T.N. Hansen, S. Techert, J.S. Wark, M. Bergh, G. Huldt, D. van der Spoel, N. Timneanu, J. Hajdu, R.A. Akre, E. Bong, P. Krejciak, J. Arthur, S. Brennan, K. Luening, J.B. Hastings, *Science* 308 (2005) 392–395.
- [10] S. Williamson, G. Mourou, J.C.M. Li, *Phys. Rev. Lett.* 52 (1984) 2364–2367.
- [11] A.A. Ischenko, L. Schäfer, J.Y. Luo, J.D. Ewbank, *J. Phys. Chem.* 98 (1994) 8673–8678.
- [12] M. Aeschlimann, E. Hull, J. Cao, C.A. Schmuttenmaer, L.G. Jahn, Y. Gao, H.E. Elsayedali, D.A. Mantell, M.R. Scheinfein, *Rev. Sci. Instrum.* 66 (1995) 1000–1009.
- [13] J.C. Williamson, J. Cao, H. Ihee, H. Frey, A.H. Zewail, *Nature* 386 (1997) 159–162.
- [14] J. Cao, H. Ihee, A.H. Zewail, *Proc. Natl. Acad. Sci. USA* 96 (1999) 338–342.
- [15] H. Ihee, V.A. Lobastov, U.M. Gomez, B.M. Goodson, R. Srinivasan, C.Y. Ruan, A.H. Zewail, *Science* 291 (2001) 458–462.
- [16] R.C. Dudek, P.M. Weber, *J. Phys. Chem. A* 105 (2001) 4167–4171.
- [17] J. Cao, Z. Hao, H. Park, C. Tao, D. Kau, L. Blaszczyk, *Appl. Phys. Lett.* 83 (2003) 1044–1046.
- [18] B.J. Siwick, J.R. Dwyer, R.E. Jordan, R.J.D. Miller, *Science* 302 (2003) 1382–1385.
- [19] C.Y. Ruan, V.A. Lobastov, F. Vigliotti, S.Y. Chen, A.H. Zewail, *Science* 304 (2004) 80–84.
- [20] W. Kaiser, *Ultrashort Laser Pulses: Generation and Applications*, Springer, Berlin, 1993.
- [21] K. Sokolowski-Tinten, C. Blome, C. Dietrich, A. Tarasevitch, M.H. von Hoegen, D. von der Linde, A. Cavalleri, J. Squier, M. Kammler, *Phys. Rev. Lett.* 87 (2001) 225701.
- [22] J.C. Williamson, A.H. Zewail, *Chem. Phys. Lett.* 209 (1993) 10–16.
- [23] H.J. Zeiger, J. Vidal, T.K. Cheng, E.P. Ippen, G. Dresselhaus, M.S. Dresselhaus, *Phys. Rev. B* 45 (1992) 768–778.
- [24] J.H. Hodak, A. Henglein, G.V. Hartland, *J. Chem. Phys.* 111 (1999) 8613–8621.
- [25] H. Park, S. Nie, X. Wang, R. Clinite, J. Cao, *J. Phys. Chem. B* 109 (2005) 13854–13856.
- [26] G. Tas, H.J. Maris, *Phys. Rev. B* 49 (1994) 15046–15054.
- [27] G.A. Garrett, T.F. Albrecht, J.F. Whitaker, R. Merlin, *Phys. Rev. Lett.* 77 (1996) 3661–3664.
- [28] C. Thomsen, J. Strait, Z. Vardeny, H.J. Maris, J. Tauc, J.J. Hauser, *Phys. Rev. Lett.* 53 (1984) 989–992.
- [29] D.R. Lide, *CRC Handbook of Chemistry and Physics*, 82nd ed., Chemical Rubber Company, Cleveland, OH, 2001.
- [30] C. Thomsen, H.T. Grahn, H.J. Maris, J. Tauc, *Phys. Rev. B* 34 (1986) 4129–4138.
- [31] A.M. Lindenberg, I. Kang, S.L. Johnson, R.W. Falcone, P.A. Heimann, Z. Chang, R.W. Lee, J.S. Wark, *Opt. Lett.* 27 (2002) 869–871.
- [32] L. Reimer, *Transmission Electron Diffraction*, fourth ed., Springer, Berlin, 1997.
- [33] L. Reimer, *Scanning Electron Microscopy*, fourth ed., Springer, Berlin, 1985.
- [34] S.I. Anisimov, B.L. Kapeliovich, T.L. Perel'man, *Zh. Eksp. Teor. Fiz.* 66 (1974) 776 [*Sov. Phys. JETP* 39, 375 (1974)].
- [35] E.D. Palik, *Handbook of Optical Constants of Solids*, Academic Press, New York, 1985.
- [36] D.S. Ivanov, L.V. Zhigilei, *Phys. Rev. B* 68 (2003) 064114.
- [37] C.J.K. Richardson, J.B. Spicer, *Appl. Phys. Lett.* 80 (2002) 2895–2897.
- [38] B. Rethfeld, K. Sokolowski-Tinten, D. von der Linde, *Phys. Rev. B* 65 (2002) 092103.
- [39] E.N. Glezer, Y. Siegal, L. Huang, E. Mazur, *Phys. Rev. B* 51 (1995) 6959–6970.
- [40] C. Guo, G. Rodriguez, A. Lobad, A.J. Taylor, *Phys. Rev. Lett.* 84 (2000) 4493–4496.